Structural Investigation of Crystalline Host Phosphor Cadmium Tellurite Systems

Rosli Hussin[1],*, Ng Siang Leong[1] and Nur Shahira Alias[1]

[1] *Phosphor Research Unit, Jabatan Fizik, Fakulti Sains, Universiti Teknologi Malaysia, 81310 UTM Skudai, Johor.*

* Author to whom correspondence should be addressed; E-mail: rbh@dfiz2.fs.utm.my

ABSTRACT

Generally, the luminescent properties of phosphors are strongly dependent on the crystal structure of the host materials. Finding a stable crystal structure, high physical and chemical stability of crystalline matrix is still a critical step to obtain rare-earth ions or transition metal ions-doped persistent phosphor with excellent properties. The glass-ceramic materials based on cadmium tellurite developed for stable host phosphor is reported in this paper. The structure of TeO_2 and CdO-TeO_2 system has been investigated by means of FT-Raman, Infrared (IR) spectroscopy and x-ray diffraction (XRD) spectroscopies. Cadmium tellurite system were prepared with the compositions of $xCdO$-$(1-x)TeO_2$ with $0.1 \leq x \leq 0.5$ in percent molar ratio, doped with 1% mol MnO_2, using solid state method. The x-ray diffraction measurement results showed that the phase in the cadmium tellurite system matched quite well with the standard ICDD files, indicating that the phases present in this sample appeared to be a phase of α-TeO_4 trigional bipyramid (tbp), $CdTe_2O_5$ and $CdTeO_3$. The Raman and Infrared spectra show that the structures are mainly builds by TeO_4 (tbp) groups, TeO_{3+1} trigional pyramid (tp) and TeO_3 (tp), while Cd^{2+} ions play as network modifiers. As addition concentration of CdO increases, TeO_4 (tbp) groups progressively change polymerized framework structure in TeO_4 (tbp) into TeO_{3+1} trigional pyramid (tp) and TeO_3 (tp). On the contrary, the addition of 1 mol % MnO_2 into the sample did not giving any effect on the structural of the final samples.

| Host phosphor I X-ray diffraction I Infrared spectroscopy I Raman spectroscopy I Tellurite glasses |

1. Introduction

Photoluminescent material with long afterglow is a kind of energy storage material that can absorb both the ultraviolet (UV) and visible lights from the sunlight and gradually release the energy in the darkness at a certain wavelength. These phosphors have been studied for a long time [1]. The properties of photoresistance and chemical stability, great brightness, long duration, no radiation and environmental capability result in their wide applications in many fields such as safety indication, lighting in emergency, instrument in automobile, luminous paint and optical devices.

Till now, the most efficient long afterglow phosphors are still based on alkaline-earth aluminates [2], silicates [3] and sulfides [4]. The persistent luminescence of ZnS-based materials-doped Cu or Mn materials is not bright enough, and the afterglow time is short, and the materials are sensitive to the humidity. Sulfide will

absorb the moisture from the surrounding environment to form sulfate that causes the destruction of sulfide lattice, and thus the material no longer shows long afterglow. As for the practical applications, even the alkaline earth aluminates have been found too sensitive to moisture despite their luminescence properties being much superior conventional ZnS:Cu materials. Silicates are suitable hosts of phosphors because of their high physical and chemical stability, especially their excellent water-resistant property but need relatively high firing temperatures.

Almost all good inorganic phosphors consist of a crystalline "host material" in which small amounts of certain impurities, the "activators" are dissolved. The activators are primarily responsible for the luminescence. Other impurities, the "co-activators" are necessary in some cases to dissolve the activator impurities into the host crystal [1]. Generally, the luminescent properties of phosphors are strongly dependent on the crystal structure of the host materials. Finding a right matrix is still a critical step to obtain rare-earth ions or transition metal ions-doped phosphor with excellent properties [5-7].

In recent years, many new phosphors based on different hosts are actively investigated, but the progress in developing the persistant phosphors with excellent lighting properties is still slow due to the lack of the suaitable host and mechanisms of long afterglow [7]. Tellurite in general are good candidates for many technological applications. These materials have a low melting temperature (~800-950 °C), are not hygroscopic, have low glass transformation temperature ($\leq 400^{o}C$) , high dielectric constant, high thermal expansion coefficient, and high optical transmission in the infrared region [8-13]. Moreover, these glasses are typically of high density, and high refractive index [14]. These properties, due to the high polarisability of Te^{4+} ions (with a solitary electron pair $5s^2$), can be even more enhanced by means of the incorporation of other heavy metals oxides that can be easily polarized (e.g. Bi^{3+}, Pb^{2+}) or with empty d orbital (Ti^{4+}, Nb^{5+}). Apart from these special optical properties, other advantages of such material will be promising candidates for luminescent hosts materials since they have stable crystal structure, high physical and chemical stability and their ability to host different rare earth or transition metal ions.

Transition metal ions eg. Mn^{2+}, have been widely used in luminescent materials. The emission can be either in green or red region depending on the host matrix because of the sensitivity of the d–d transition in Mn^{2+} to the crystal field [15]. However, to the best of our knowledge, the luminescence properties Mn^{2+} in cadmium tellurite system has not yet been reported as a long-lasting phosphor materials so far. Cadmium tellurite matrices systems are attractive host materials for the study of development of advanced phosphors due to low melting point, high thermal stability and good rare-earth or transition metal ions solubility.

The aim of this work is to report the suitable crystalline phase composition and its structure present in cadmium tellurite system which can be used as stable host lattices phosphor through x-ray diffraction (XRD), infrared (IR) and Raman spectroscopic studies. It is important to find stable host in which different emission wavelengths can be obtained by doped with different concentration of Mn^{2+} ions. So the tellurite based materials with long afterglow properties with new crystalline structures are necessary to be developed.

2.   Experimental Procedures

Sample Preparation

Cadmium tellurite samples were prepared with the compositions of $xCdO-(1-x)TeO_2$ doped with 1 mol% MnO_2, where x =0.1 to 0.5 in molar ratio, using the conventional solid state method. All chemicals used were reagent grade of MnO_2 (Sigma), $CdCO_3$ and TeO_2 (Aldrich). The stoichiometric compositions of the batch materials (10 g) were thoroughly mixed and milled in an agate mortar and then heated in a alumina crucible at temperatures in the range of 900–950°C for about half an hour in an electrically furnace in air atmosphere. The

furnace was switch off and the samples was leftout until it cool at room temperature before removed from the furnace.

Characterization

The structure of the prepared samples was analyzed by means of X-ray diffraction measurements (XRD), using powders. The XRD measurements were carried out with CuK_α radiation at room temperature using Siemens Diffractometer D5000, equipped with diffraction software analysis. The diffraction spectral data were collected at constant (2θ) steps of 0.04^o, where 2θ from 10 to 80°, and dwell of 4s. The d-spacings obtained were compared with those in the literature in an attempt to identify the crystal phases formed. As reference the latest database of ICDD (International Center for Diffraction Data, ICDD) was also used.

The infrared (IR) spectra have been recorded using a Perkin-Elmer Spectrum One FT-IR spectrometer from 2000 to 400 cm^{-1} at intervals of 4 cm^{-1}. There were no characteristic absorption bands in the range of 4000 – 1300 cm^{-1} for the samples. Hence the spectra are presented for the region of 1200–400 cm^{-1} in this work. Measurements were carried out on dispersed in pressed KBr pellets containing the same weight of the powder samples to enable us to roughly compare the relative intensities of the bands.

The Raman spectra were measured with a Perkin-Elmer Spectrum GX spectrometer in the spectral range 100–1200 cm^{-1}. The sample was excited with an argon ion laser with power of about 200 mW. The spectrum was observed in the quasi-back scattered mode. The digital intensity data were recorded at intervals of 4 cm^{-1} and the spectral resolution was about 4 cm^{-1}.

3.   Results

XRD Patterns

Fig. 1 shows the XRD patterns from all of the samples as formed in $xCdO-(1-x)TeO_2$ system. All the obtained samples were fully crystalline. The diffraction patterns of the crystalline phases formed on cooling were identified as crystalline paratellurite α-TeO_2 (ICDD: 42-1365), $CdTe_2O_5$ (ICDD: 24-0169), $CdTeO_3$ (ICDD: 77-1906), as summarized in Table 1.
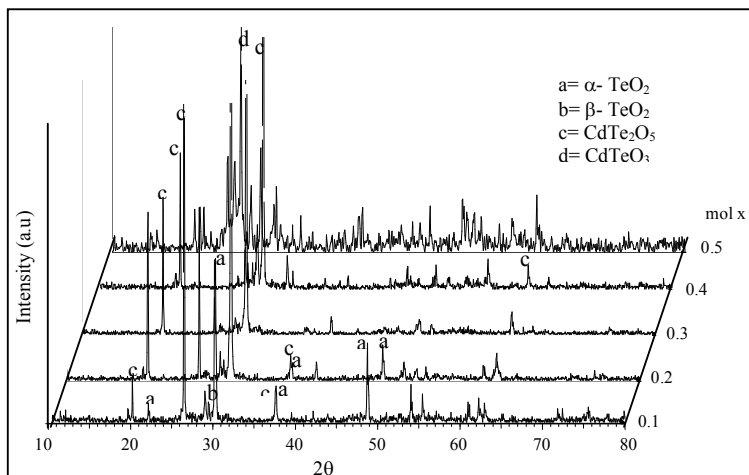
Figure 1: X-ray diffraction (XRD) patterns of $xCdO-(1-x)TeO_2$ system, with $0.1 \leq x \leq 0.5$.

Table 1: Composition of the samples $xCdO$-$(1-x)TeO_2$ and it identify crystalline phase.

| Composition		Phase
CdO	**TeO₂**	
0.1	0.9	α-TeO_2 (m), $CdTe_2O_5$(mn)
0.2	0.8	α-TeO_2 (m)*, $CdTe_2O_5$ (mn)
0.3	0.4	$CdTe_2O_5$ (m), $CdTeO_3$ (mn)
0.4	0.6	$CdTe_2O_5$ (m), $CdTeO_3$(mn)
0.5	0.5	$CdTeO_3$ (m), $CdTe_2O_5$ (mn)

Note: m – major phase, mn- minor phase,
* Reduce to 90% based on comparison between highest peak.

Raman Spectra

Raman spectra of the α, β and γ-TeO_2 powder, along with $xCdO$-$(1-x)TeO_2$ samples are presented in Fig. 2. Raman vibration frequencies are summeried in Table 2. Raman spectra of 10CdO-90TeO₂–glass is rather similar to α-TeO_2 data including the typical broadening observed in glasses, consist of major bands in the 600–800 cm cm^{-1} range and a broad band around 490 cm cm^{-1}. The typical broadening of the vibration bands due to the glassy state is observed. The Raman spectrum of the glass matrix presents six bands at: 748, 626, 533, 406, 288 and 140 cm^{-1} (Fig. 1).

The α-TeO_2 spectrum presented in Fig. 2 is dominated by two bands at 647 and 392 cm^{-1}. Smaller features are observed at 158, 175, 339, 591, 718, 721 and 767 cm^{-1}. Maximum positions were measured with ± 5 cm^{-1} accuracy. α-TeO_2 belongs to the D_4^4 space group and the Raman bands are assigned following the work by Pine and Dresselhaus [16]. In this way the bands with the largest amplitudes at 392 and 647 cm^{-1} are assigned to the $v_2(A_1) = (v_sTeO_{2ax})$ and $\upsilon_1(A_1) = \upsilon_sTeO_{2eq}$ vibrational mode. δ_1, δ_2, v_{as}(Terminal Oxygen, TeO_{ax}) and $v_{as}(TeO_{2eq})$ modes are related to the smaller bands at 591, 718, 721 and 767 cm^{-1}, respectively. The structure of α-TeO_2 is built of (TeO_4) trigonal bipyramids (tbp) connected at the vertices and the two bands at 392 and 647 cm^{-1} have been assumed to be due to this structure. Spectra for samples x=0.1, 0.2 and x=0.3 in the larger TeO_2 content part of the phases in Fig. 2 are assumed to be an envelope of the crystalline α-TeO_2 spectrum, assigned to vibrations of (TeO_4) species. As we go further from x=0.3 to x=0.4 part in the samples, these bands diminish in amplitude at the expense of an increase in amplitude of the component at 724 cm^{-1}. This last band is assigned to (TeO_3) trigonal pyramids (tp) and is due to the breakdown of the initially fully polymerized structure occurring with the addition of cadmium oxide. From sample x=0.4 and 0.5, the addition of CdO is followed by the appearance of a completely new band, in the 724 cm^{-1} region which is the same as that for TeO_3 bonds in Na_2TeO_3 groups [17] and $ZnTeO_3$ [18,19]. This Raman spectra is similar with β-TeO_2.

The Raman spectra were also exhibited two main peaks at around ~650 and ~730 cm^{-1}. The relative intensity of the 730 cm^{-1} peak due to TeO3+1 units against the 650 cm^{-1} peak intensity due to the TeO4 tbp decreases with CdO content. From these results the addition of an intermediate oxide is assumed to develop the TeO3 entities. The Raman bands around 650 and 730 cm^{-1} are assigned to stretching vibrations in TeO_4 and TeO_3 and/ or TeO_{3+1} groups, respectively. The increase in intensity observed for the 730 cm^{-1} band with CdO concentration. The dominant three-dimensional network structures in the glassy mixture of (10CdO-90TeO₂) are triagonal pyramidal TeO_3 with minor features of short range of distorted tbp TeO_4 in which a tbp TeO_4 unit is linked together by Te_{ax}–O–Te_{eq} bridges to form a primary bridged tetrahedral unit of Te_2O_7 (TeO_{3+1}), leading to a structure of infinite chain. Therefore, 10CdO-90TeO₂ sample experience structural changes from TeO_4 (tbp); Te_2O_7 (TeO_{3+1})or TeO_3 when doped with CdO.
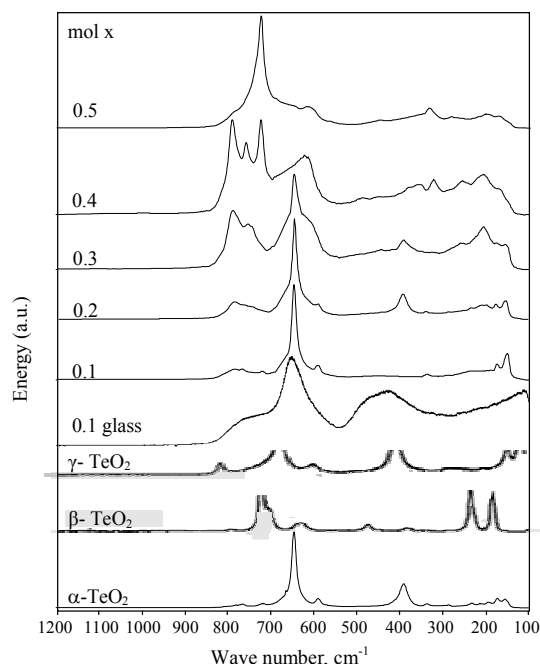
Figure 2: Raman spectra of the different polymorph of α, β, γ-TeO$_2$ and samples xCdO-(1-x)TeO$_2$ system, with 0.1≤x≤0.5.

Table 2: Raman characteristic frequencies of crystalline TeO$_2$ and xCdO-(1-x)TeO$_2$ system, with 0.1≤x≤0.5.

	δ (Te-O-Te)	δ (TeO$_3^{2-}$)	υ$_s$(Te-O-Te)	υ$_{as}$TeO$_4$	υ$_{s1}$TeO$_4$	υ$_s$(Te-O$^-$)	υ$_{s2}$TeO$_4$	υ$_s$(TeO$_3^{2-}$)
α-TeO$_2$	158,175,339		392*	591	647*	721	767	
β-TeO$_2$	234, 336		450	595	673	740*		
γ-TeO$_2$			426		680*		820	
x=0.1	151,175,	339	-	594	647*	722	767	785
0.2	155,175,	339	393	592	648*		765	788
0.3	156,177,207		392,445	611	647*		754	789*
0.4	169,207	257,323,357	490		623*	724*	759	791*
0.5	156,175,203	262,283,336	454	613	629	724*		793

Note: Sh- shoulder, *- main peak (sharp and highest)

The Raman frequencies of crystalline TeO$_2$ observed around 150 to 350 cm^{-1} are due to the oscillations of the metal cation (Te) in its oxygen cavities of the TeO$_4$ tetrahedra [19]. These bands are a characteristic feature of tetragonal TeO$_2$ [20-21]. The bands around 188, 219-223, 266-270, and 343-350cm^{-1} observed in the spectra of samples containing up to 50 mol% (Fig. 2) correspond to the vibrational modes of the TeO$_4$ tetrahedra [21]. The great similarity between these spectra and the spectrum of crystalline TeO$_2$ suggests that the short range structure of these sample is a ordered version of tetragonal TeO$_2$ with TeO$_4$ trigonal bipyramids structural units [13]. The Raman spectra also shown that the sample does not have either free OH or hydrogen bonded OH groups, due to the absence of stretching (3150–3500 cm^{-1}) and bending modes (1650–1750 cm^{-1}) of hydroxyl group [23,24]. In order to complete this Raman structural approach, we have also undertaken an investigation by infrared spectroscopy.

FT-IR spectra

The FT-IR spectra of of xCdO-(1-x)TeO$_2$ system, with 0.1≤x≤0.5 and crystalline α-TeO$_2$ the present investigation are shown in Fig. 3. The characteristic IR frequencies of crystalline TeO$_2$ and the samples are summarized in Table 3. It can be seen that each spectrum consists of a major band in the range of 600–800 cm^{-1}. This band was mainly assigned to vibrations due to tellurium–oxygen polyhedra in line with assignments by [25]. The spectrum of crystalline TeO$_2$ shows two net peaks at 780 and 675 cm^{-1} and a shoulder at about 635 cm^{-1}. These bands correspond respectively to the symmetric axial $v_2(A_1) = (v_sTeO_{2ax}) = 635$cm^{-1}, vibration of the continuous networks composed of TeO$_4$ tetragonal bipyramids (tbp), and the symmetric equatorial $\upsilon_1(A_1)= \upsilon_sTeO_{2eq} = 780$ cm^{-1} (sharp) vibrational modes of the TeO$_4$ tetrahedral units [26]. The band around 675 ($\upsilon_6(B_2)= \upsilon_{as}TeO_{2ax}$) and 714 cm^{-1} ($\upsilon_8(B_1)= \upsilon_{as}TeO_{2eq}$) is assigned to antisymmetric vibrations of Te–O–Te linkages constructed by two unequivalent Te–O bonds [26].
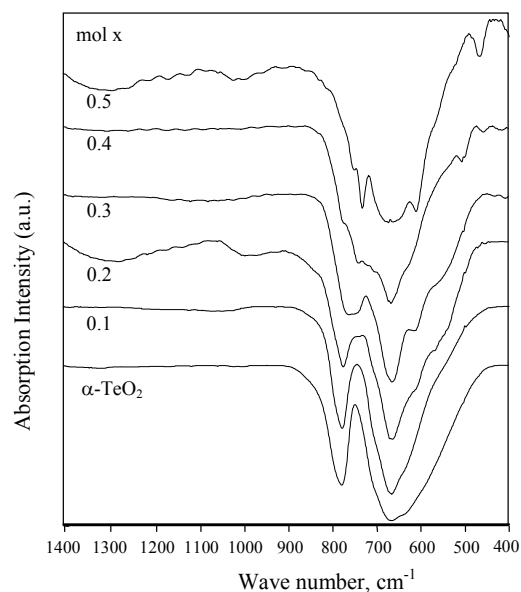
Figure 3: FTIR spectra of xCdO-(1-x)TeO$_4$, with 0.1≤x≤0.5 doped 1 mol% MnO$_2$ and α-TeO$_2$ crystalline samples.

Table 3: IR characteristic frequencies of crystalline TeO$_2$ and xCdO-(1-x)TeO$_2$ system, with 0.1≤x≤0.

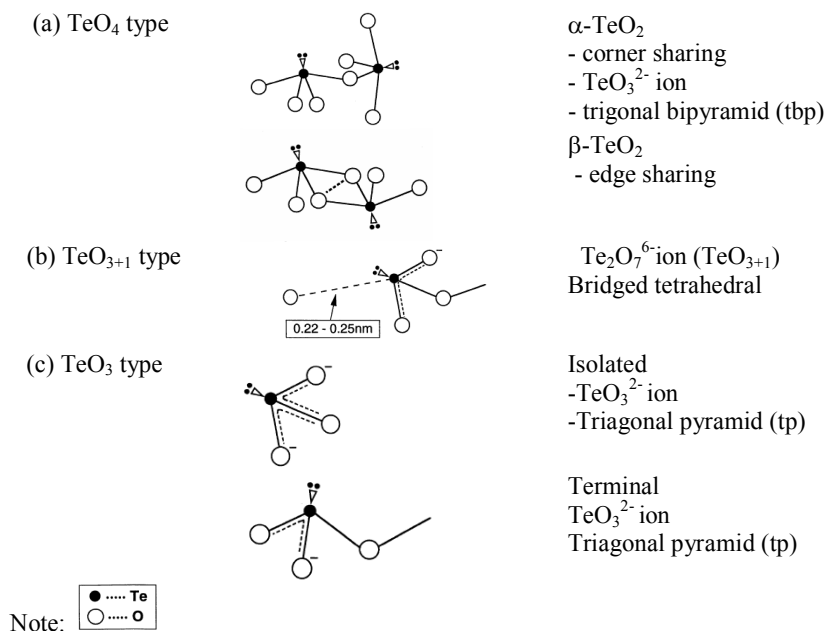|		υ_sTeO_{2ax}	$\upsilon_{as}TeO_{2ax}$	$\upsilon_{as}TeO_{2eq}$	υ_sTeO_3	υ_sTeO_{2eq}
α-TeO$_2$		635sh	675	714		780
x=0.1	545sh	647sh	663	695		774
0.2	565sh	615sh	660	694		772
0.3	558sh	607	660		750,768	
0.4	505	637	664		737	770
0.5	464,548sh	610	660	729	749,765sh	

Note: Sh- shoulder

4. Discussion

At ambient conditions, TeO_2 is known to exist in the two polymorphous forms, paratellurite, α-TeO_2 [19-21] and tellurite, β-TeO_2 [26], the constitution of TeO_2 system was always unambiguously related to one of them, namely, to the former structure. In those units, the two Te–O bonds have lengths of about 1.87 Å and form the angle 103°, which is rather close to the atomic arrangement in the isolated TeO_2 molecule [26]. In the lattice, the molecules are packed so that every atom of Te has the two new neighboring oxygen atoms separated from him for about 2.12 Å. Thus, with the four nearest oxygen atoms, each Te atom builds a TeO_4 polyhedron in view of a trigonal bipyramid, called disphenoid. Its 'axis' is formed by the two long Te–O bonds, whereas the equatorial plane includes the two short Te–O molecular bonds and the $5s^2$ lone electron pair of Te. These short bonds are called '*equatorial*', and the long ones '*axial*'. According to the recent first principles calculations [25], the bond orders have values of 1.7 and 0.3 for those two bonds, respectively. Therefore, the first of them (1.87 Å) can be classified as mainly covalent, whereas the second one (2.12 Å) most likely has largely electrostatic nature, and result from the dipole–dipole intermolecular interactions. In both structures, tellurium atoms have four neighbouring oxygen atoms and the basic structural unit is a TeO_4 disphenoid, or if we take into account the $5s^2$ lone pair of tellurium atoms (E), a distorted TeO_4E bipyramid. In this bipyramid, the two *equatorial* oxygen atoms are separated from Te by distances shorter than the sum of the covalent radii of O (0.73A°) and of Te (1.35A°), and the two *axial* oxygen atoms by distances longer than that value (Fig. 4).
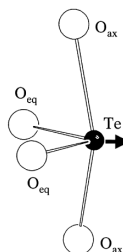

Figure 4: Basic structural unit for the TeO_4 present in α- and β-TeO_2. [17,23]

The local structure around Te atoms has been classified into five groups based on the structural units present in tellurite crystals as illustrated in Fig. 5. These are (1) TeO_3 type which consists of an isolated TeO_3 type and a terminal TeO_3 type, (2) TeO_{3+1} type and (3) TeO_4 type which consists of an α-TeO_2 type and a β-TeO_2 type. An isolated TeO_3 type means that the TeO_3 tp structural unit is present as a free anion; the terminal TeO_3 type means that the TeO_3 tp has one corner which is connected with a neighboring TeO_n polyhedron; the TeO_{3+1} type means that the TeO_3 tp has an additional O atom at a remote distance from 0.22 to 0.25 nm. Furthermore, the α-TeO_2 type contains TeO_4 tbp structural units which are connected by sharing their corners, and the β-TeO_2 type contains Te_2O_6 units consisting of two edge-shared TeO_4 tbps. Three structural $TeOn$ entities have been reported (Fig.1): first a TeO4 somewhat trigonal bipyramid (tbp) group with two axial and two equatorial oxygen atoms (the third equatorial position of the sp^3d hybrid orbitals is occupied by the lone pair); second, a TeO3+1 asymmetric polyhedron in which one Te–O axial bond shortens while the other elongates; third, a TeO3 trigonal pyramid (tp) with three short Te–O distances. TeO4 and TeO3 entities look like the tellurium oxygenated environment existing, respectively, in the crystal of α-TeO2 and ZnTeO3. Therefore these crystalline phases were used as reference samples. In α-TeO2 the distorted tbp TeO4 exhibits two axial Te–Oax bonds (2.08 A°) and two equatorial Te–Oeq bonds (1.90 A°), while the Te environment in ZnTeO3 is a tp TeO3 with a mean Te–O distance equal to 1.876 A°.

(a) TeO$_4$ type

α-TeO$_2$
- corner sharing
- TeO$_3^{2-}$ ion
- trigonal bipyramid (tbp)

β-TeO$_2$
- edge sharing

(b) TeO$_{3+1}$ type

Te$_2$O$_7^{6-}$ion (TeO$_{3+1}$)
Bridged tetrahedral

0.22 - 0.25nm

(c) TeO$_3$ type

Isolated
-TeO$_3^{2-}$ ion
-Triagonal pyramid (tp)

Terminal
TeO$_3^{2-}$ ion
Triagonal pyramid (tp)

Note: ● ····· Te
        ○ ····· O

Figure 5: Illustration of the structural models of TeO$_4$ type. [23]

Conventionally, the α and β-TeO$_2$ structures are described as frameworks of these TeO$_4$ units, packed in such a way that each oxygen atom is coordinated to two tellurium atoms thus forming a *highly asymmetric* bridge Te$-_{ax}$O$_{eq}$–Te (Fig. 6(a) and (b)). In the α-TeO$_2$ structure, TeO$_4$ units constitute, by sharing corners, the three-dimensional network visualised in Fig. 6(a). In the β-TeO$_2$ structure, they share, alternately, corners and edges and so constitute a two-dimensional network sheets in Fig. 6(b). The structures are regarded as consisting of symmetric Te–O–Te bridges in which bonds are chemically identical.

(a)   (b)
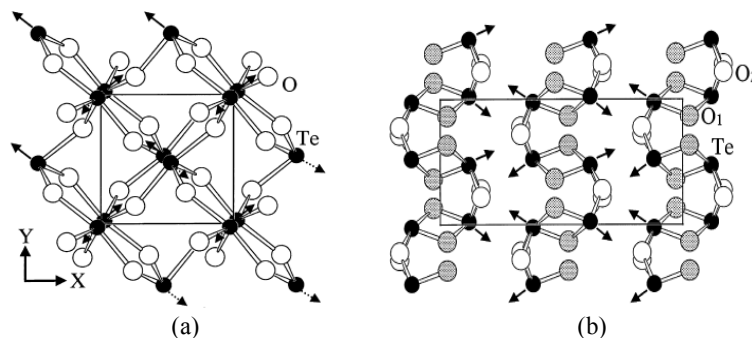
Figure 6: Structures of the different TeO$_2$ crystalline polymorphs: (a) the xy projection of the α-TeO$_2$ lattice; *corner sharin*g (b) the β-TeO$_2$ lattice projection showing its layer structure, *edge sharing*. (arrows indicate the position of lone electron pairs of Te). (This figure is taken from Ref. [20])

In the paratellurite lattice (α-TeO$_2$ structure), the TeO$_2$ molecules frame the spiral-like tunnels so that the lone pairs of Te-atoms are always oriented inside them, and two TeO$_4$ neighbouring disphenoids are

interconnected via a common corner without having common O–O edges (Fig. 6(a)). The concept of the TeO_4 disphenoids as its basic units suggests that the paratellurite lattice is the 3D-framework, made of the bent Te–O–Te bridges considered as homologues to the Si–O–Si bridges in the quartz lattice. In this connection it is useful to recall some general features inherent for the Raman spectra of such lattices. The middle-frequency and the highest-frequency parts of the spectra are associated with the displacements of the oxygen atoms, and can be described in terms of localized stretching vibrations of the Te–O–Te bridges. The Raman intensity of the asymmetric Te–O–Te stretching vibrations (occupying the highest frequency range) is related to the difference in the electronic polarizability properties of the two bonds involved on the Te–O–Te bridge. Consequently, if the bonds are identical, those vibrations would have a vanishing intensity in the Raman spectra. Contrary to this, the symmetric Te–O–Te stretching vibrations lying in the middle-frequency part of the spectrum would produce the strongest lines.

The β-TeO_2 lattice (tellurite) [26] is also made from the TeO_4 disphenoids (Fig. 6(b)), but its constitution is essentially other. In contrast to α-TeO_2, the disphenoids in β-TeO_2 are adjusted alternatively by their corners and edges, and the nearest atoms of Te are linked via two Te_{ax}–O_{eq}–Te bridges (which can be called double bridges [19-21]), thus framing a sharply pronounced anisotropic (layer) structure.

These studies have revealed two basic findings. First, pure TeO_2 consists of TeO_4 trigonal bipyramids (tbp) in which one equatorial site of the sp^3d hybrid orbitals is occupied by a lone pair of electrons and the other two equatorial and axial sites are occupied by oxygen atoms. Second, addition of CdO modifiers into the TeO_2 network causes a change of the Te coordination polyhedron from TeO_4 tbp to TeO_3 trigonal pyramid (tp) in which one of the Te sp^3 hybrid orbitals is occupied by a lone pair of electrons; this transformation causes also an increases in the number on non-bridging oxygen (NBO) atoms.

The basic structural unit of the tellurite glass is made up of a $[TeO4]$ trigonal bipyramid (tbp) with one of the equatorial positions occupied by a lone pair of electrons. A network modifier/glass-former causes the change in coordination of Te atom from TeO4 tbp line structure of α-TeO_2 (tetragonal) and that of β-TeO_2 (tetragonal) are different from each other.

The Raman spectra of the α- and β-TeO_2 lattices (Fig. 2(a) and (b)) are clearly dominated by the strong high–frequency stretching vibrations, and have rather weak lines in the middle-frequency part. Thus, the presence of the largely covalent terminal Te–O bond is unequivocally manifested there, whereas none of the lines in those spectra indicates the existence of Te–O–Te bridges made of such bonds. Therefore, from the objective spectrochemical point of view, the α- and β-TeO_2 lattices cannot be considered as a classic framework, but rather as island-type ones, i.e. those built up from the quasi isolated TeO_2 molecules whose synchronous vibrational are account for the high frequency strongest bands in Fig. 2(a) and (b).

The vibrational spectrum of inorganic solid materials could be studied on the basis of isolated and repeated structural units [19-27]. Therefore, the structural studies for triagonal bipyramid TeO_4^{2-}($C2v$) and bridged tetrahedral TeO_{3+1} have been found effective to characterize the structural features of tellurite system using Raman measurements comparable with infrared method [19-27]. Spectroscopic investigations have shown that CdO-TeO_2 systems are formed by a three-dimensional network composed of asymmetrical TeO_4 trigonal bipyramids (tbps) when the CdO content is relatively low. An increase in the CdO concentration leads to the progressive formation of distorted TeO_3 or TeO_{3+1} units (where the subscript "3 + 1" indicates the existence of a longer bond compared to the three others, followed by the creation of regular trigonal TeO_3 pyramids (tps) associated with non-bridging oxygen atoms (NBO). As known, tellurite glasses follow the pattern of crystalline α-TeO_2, which are formed by $[TeO_4]$ groups as trigonal bipyramids (tbp) [21]. In tellurite glasses, such structural units can progressively form $[TeO_{3+1}]$ and trigonal pyramids $[TeO_3]$ (tp) when the glass network becomes more open and non-bridging oxygens are created due to the incorporation of CdO ions.

5. Conclusion

Cadmium tellurite in the system $CdO-TeO_2$ doped with 1 mol% MnO_2 were prepared by solid state method. XRD, IR and Raman spectroscopies have been used in order to approach the structure of $CdO-TeO_2$ system. The presence of CdO showed additional Raman bands at about ~790 cm^{-1} apart from the normal bands for crystalline phase of tellurite. The addition of more CdO suppressed the creation of more TeO_3 tp units. There established a trade of between TeO_4 tbp and TeO_3 tp units due to the presence of $CdTeO_3$. The XRD patterns confirm Cd_2TeO_5 and $CdTeO_3$ phase in the investigated system up to 40 mol% CdO. The vibrational spectra evidenced that the main structural units are Cd_2TeO_5 and $CdTeO_3$, followed same trand in XRD patterns. These glasses present characteristic tellurium atoms coordination changes, with the CdO content, from TeO_4E through $TeO_{3+1}E$ to TeO_3E units with NBO. Increasing the concentration of cadmium oxide, (TeO_3) units are produced as a result of depolimerization processes. CdO oxide transforms the tellurite network assuming to act as a network modifier. The addition of low concentrations 1% MnO_2 is insufficient to break the weak non-equivalent Te-O bond in the TeO_4 building unit. Spectroscopic properties indicate that these system are potential hosts for presistent phosphor and the photoluminesce study of these material is in progress.

6. Acknowledgments

7. References

[1]   G. Blasse, B.C. Grabmaier, Luminescent Materials, Springer, Berlin, 1994.
[2]   E. Nakazawa and T. Mochida, Journal of Luminescence, 72&74 (1997) 236.
[3]   Tuomas Aitasalo, Dariusz Hreniak, Jorma Holsa, Taneli Laamanen, Mika Lastusaari, Janne Niittykoski, Fabienne Pelle, Wieslaw Strek, Journal of Luminescence, 122&123 (2007)110.
[4]   M. Bredol, J. Merikhi, C. Ronda, Ber. Bunsen-Ges. Phys. Chem. Chem. Phys. 96 (1992) 1770.
[5]   Y. Lin, C.W. Nan, X. Zhou, J. Wu, H. Wang, D. Chen, S. Xu, Mater. Chem. Phys. 82 (2003) 860.
[6]   T. Aitasalo, P. Deren´, J. Holsa, H. Jungner, J.C. Krupa, M. Lastusaari, J. Legendziewicz, J. Niittykoski, W. Strek, J. Solid State Chem. 171 (2003) 114.
[7]   J. Holsa T. Aitasalo, H. Jungner, M. Lastusaari, J. Niittykoski, G. Spano, J. Alloys Comp. 374 (2004) 56.
[8]   B.C. Sales, Mater. Res. Soc. Bull. 12 (1987) 32.
[9]   F.L. Galeener and J.C. Mikkelsen Jr., Solid State Commun. 30 (1979) 505.
[10]   S.W. Martin, Eur. J. Solid State Chem. 28 (1991) 163.
[11]   D.R. Tallant, C. Nelson and J.A. Wilder, J. Phys. Chem. Glasses 27 (1986) 71.
[12]   Y. Himei, Y. Miura, T. Nanba, A. Osaka, J. Non-Cryst. Solids 211 (1997) 64.
[13]   R. Rolli, K. Gatterer, M. Wachtler, M. Bettinelli, A. Speghini, D. Ajo, Spectrochim. Acta A 57 (2001) 2009.
[14]   M.J. Weber, J.D. Myers, D.H. Blackburn, J. Appl. Phys. 52 (1981) 2944.
[15]   S.J. Choquette, J.C. Travis, D.L. Duewer, Proc. SPIE 3425 (1998) 102.
[16]   A.S. Pine, G. Dresselhaus, Phys. Rev. B 5 (10) (1972) 4087.
[17]   T. Sekiya, N. Mochida, A. Ohtsuka, M. Tonokawa, J. Non-Cryst. Solids 144 (1992) 128.
[18]   H. Bu¨ rger, K. Kneipp, H. Hobert, W. Vogel, V. Kozhukarov, S. Neov, J. Non-Cryst. Solids 151 (1992) 134.
[19]   Nelson B.N., and Examos G.J., J. Chem. Phys. 71(1979)2739.

[20]   O. Noguera, T. Merle-Mejean, A.P. Mirgorodsky, M.B. Smirnov, P. Thomas, J.-C. Champarnaud-Mesjard, J. Non-Cryst. Solids 330 (2003) 50.
[21]   Shaltout I., Tang Y., Braunstein R. and Abu-Elazm A. M., J. Phys. Chem. Solids 56,141 (1995).
[22]   Peercy P. S. and Fritz, I. J., Phys. Rev. Left. 32, (1974). 466.
[23]   S. Sakida, S. Hayakawa, T. Yoko, J. Non-Cryst. Solids 243 (1999) 1.
[24]   J. C. Sabadel, P. Armand, P.-E. Lippens, D. Cachau-Herreillat, E. Philippot, J. Non-Cryst. Solids 244 (1999) 143.
[25]   P.A. Thomas, J. Phys. C: Solid State Phys. 21 (1988) 4611.
[26]   V.H. Beyer, Z. Kristallogr. 124 (1967) 228.
[27]   O. Noguera, M. Smirnov, A.P. Mirgorodsky, T. Merle-Mejean, P. Thomas, J.C. Champarnaud-Mesjard, J. Non-Cryst. Solids 345&346 (2004) 734.